coatings

MDPI

Article

Preparation of Wood-Based Carbon Quantum Dots and Promotion of Light Capture Applications

Yujia Fu [1,2], Hui Xu [1,2], Qiang Guo [1,2], Dongbo Yang [1,2], Yanfei Pan [1,2,*] and Zhenhua Xue [1,2,*]

[1] College of Material Science and Art Design, Inner Mongolia Agricultural University, Hohhot 010010, China; fuyujia68@163.com (Y.F.); ydbydb1022@163.com (D.Y.)
[2] Inner Mongolia Key Laboratory for Sandy Shrubs Fibrosis and Energy Development and Utilization, Hohhot 010018, China
* Correspondence: panyanfeiz@imau.edu.cn (Y.P.); x_zhenhua@126.com (Z.X.)

Abstract: CQDs are a type of fluorescent nanocarbon material that possess excellent optical properties. They have a wide range of raw material sources, making them a versatile option for various applications. The use of fluorescent materials to enhance the solar energy capture capacity of chloroplasts has the potential to significantly improve natural photosynthesis. CQDs and N-CQDs were prepared from natural Salix wood powder using a simple, green, and environmentally friendly hydrothermal method. These materials can effectively capture ultraviolet (UV) light and were used for photosynthesis to enable chloroplasts to utilize UV light that cannot be absorbed by them. The chlorophyll content of leaves treated with CQDs and N-CQDs increased, with the N-CQDs 25 mg/L treated group showing a 35.6% increase compared to the untreated group. Additionally, the treatment of CQDs and N-CQDs positively affected the transfer of electrons from photosystem II, further enhancing photosynthetic activity. This study presents ideas for expanding the use of solar energy, optimizing the photosynthesis charge transfer pathway, and improving solar energy conversion efficiency.

Keywords: wood flour; carbon quantum dots; light energy; photosynthesis; photosynthetic activity

Citation: Fu, Y.; Xu, H.; Guo, Q.; Yang, D.; Pan, Y.; Xue, Z. Preparation of Wood-Based Carbon Quantum Dots and Promotion of Light Capture Applications. *Coatings* **2024**, *14*, 417. https://doi.org/10.3390/coatings14040417

Academic Editors: Marko Petric and Philipp Vladimirovich Kiryukhantsev-Korneev

Received: 5 March 2024
Revised: 19 March 2024
Accepted: 29 March 2024
Published: 31 March 2024

1. Introduction

Over the last few decades, there has been a significant increase in energy demand owing to the swift progress of modern technology and society. To decrease reliance on non-renewable energy sources, researchers are exploring environmentally friendly and sustainable alternatives, and solar energy appears to be the most advantageous option [1,2]. However, collecting and utilizing solar energy remains a persistent challenge. On the other hand, green plants possess the ability to utilize solar energy through natural photosynthesis. They assimilate carbon dioxide (CO_2) and water (H_2O) to generate organic matter while releasing oxygen (O_2). Photosynthesis serves as the foundation for plant growth—the fundamental process critical for the preservation of Earth's carbon and oxygen cycles [3]. During natural photosynthesis, photosynthetic organisms utilize light-induced transfers of energy and electrons to power their metabolism. This process involves the capture of solar energy through photosynthetic units (PSUs), accomplished by the binding of light-harvesting complexes (LHCs), which play a key role as a light-harvesting antenna. This is followed by electron transfer to specialized chlorophyll cofactors in specialized reaction centers (RC). In this area, the energy captured is transformed into chemical energy within the chloroplasts and stored as sugar bonds [4–6]. However, plants only convert 2–4% of light into energy, and current research is focused on improving photosynthesis efficiency during plant growth. Researchers have proposed various strategies to address the key issue, including genetic improvement of the plant itself [7,8] and the artificial regulation of the plant growth cycle with supplemental light or light-converting materials [9]. Compared to the time-consuming and challenging process of genetic engineering modification [10], artificial regulation proves to be more efficient and economically beneficial. Therefore,

researchers prioritize identifying suitable materials for the artificial regulation of photosynthesis. In biotechnology, quantum dots, multifunctional fluorescent semiconductor nanomaterials with unique photophysical properties, find extensive applications [11–13]. Due to the significant potential of quantum dots as energy donors or acceptors, they are often utilized in numerous studies to regulate the light-harvesting capacity of photosynthetic organisms and enhance their photosynthetic activity and growth rate [14]. Quantum dots have become a significant research subject in the field of photosynthesis, with great potential as nanomaterials [6,15].

The development of carbon quantum dots has broadened the application of quantum dots in life sciences, such as agricultural and photosynthesis research [16]. In 2004, Xu et al. from Clemson University [17] discovered carbon quantum dots (CQDs) by accident while preparing SWCNTs using electrophoresis. Carbon quantum dots are fluorescent nanocarbon materials with a particle size of less than 10 nm [18]. They offer various advantages including exceptional optical properties, water solubility, low toxicity, environmentally friendly nature, biocompatibility, easy functionalization, ample sources of raw materials, and low cost of preparation [19]. Their most visible optical features comprise robust absorption peaks in the ultraviolet (UV) region and photoluminescence; when exposed to light, good water-soluble carbon quantum dots emit bright fluorescence [20]. Using the distinctive optical features of carbon quantum dots to regulate light trapping, electron transfer, and energy conversion in photosynthesis, with the aim of enhancing plant photosynthetic efficiency, may yield outcomes that are unattainable through alternative techniques. Currently, numerous scientific research teams have explored the use of carbon quantum dots to regulate plant photosynthesis and enhance plant growth. These teams have consistently found that an appropriate amount of carbon quantum dots can increase the utilization of light energy by chloroplasts, improve photosynthesis efficiency, and facilitate carbon accumulation within plants [21].

CQDs [22] were prepared using natural Salix wood powder and citric acid as a one-step hydrothermal process for the carbon source, while N-CQDs (Nitrogen-doped carbon quantum dots) were synthesized through doping with urea. They were utilized as light-trapping materials in plant photosynthesis, respectively, with the aim of enhancing the capture and conversion efficiency of light energy by plants. Both CQDs and N-CQDs are able to absorb UV light and convert it into blue light. This mechanism enhances the efficiency of chloroplasts in harnessing light energy, ultimately leading to an increase in the chlorophyll content of photosynthetic pigments located in the leaves treated with CQDs and N-CQDs. The Hill reaction demonstrated that both CQDs and N-CQDs facilitated positive electron transfer to photosystem II, thereby enhancing photosynthetic activity. CQDs promotes chloroplast capture of light energy to enhance photosynthesis as shown in Figure 1. This study presents an extensive analysis of the impacts of CQDs and N-CQDs on the utilization of solar energy through photosynthesis in plants while suggesting strategies to broaden the usage of solar energy, enhance the charge transfer pathway of photosynthesis, and boost the efficiency of solar energy conversion.

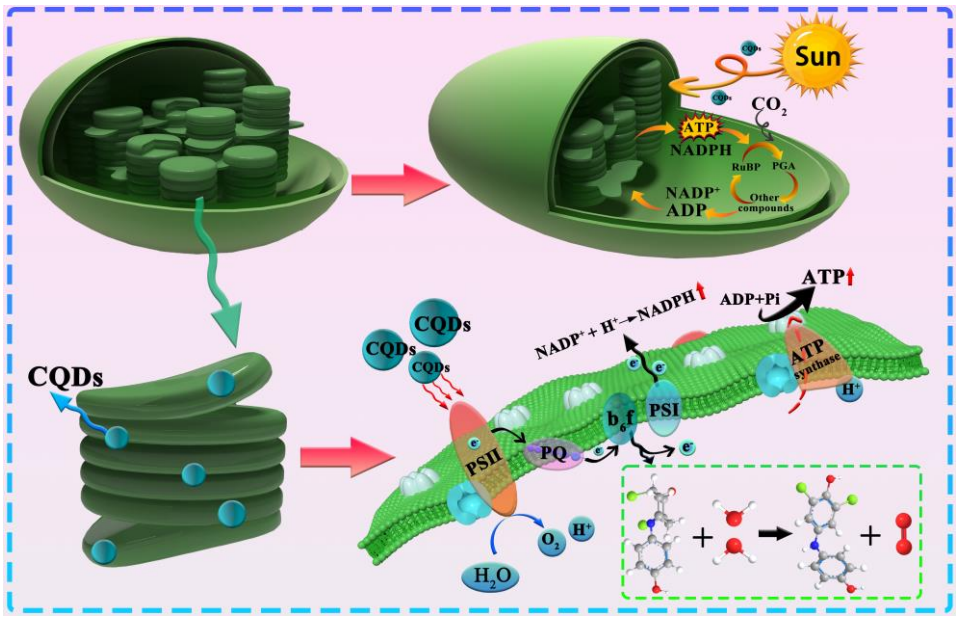

Figure 1. Schematic diagram of CQDs promoting light energy capture by chloroplasts to enhance photosynthesis.

2. Materials and Methods

2.1. Wood-Based Carbon Quantum Dot Preparation

Preparation of Carbon Dots: Salix wood powder and lignin were utilized as precursors for the hydrothermal synthesis of carbon dots. Salix wood strips were peeled, ground, and sieved to 60 mesh wood powder. The amounts 0.9, 1.1, 1.3, and 1.5 g of Salix wood powder and lignin were dissolved in 30 mL of deionized water and ultrasonically dispersed for 10 min. After sonication, the mixture was moved to a 100 mL PTFE-lined stainless-steel autoclave and underwent additional reaction at 180 °C for 12 h. The reactants underwent preliminary filtration via centrifugation at 8000 rmp for 10 min, followed by filtration through a 0.22 μm filter membrane to remove macroaggregates of wood-based CQDs. Finally, the yellow-brown liquid obtained through filtration underwent dialysis and purification in a 1000 Da molecular weight cut-off dialysis bag filled with deionized water for 48 h. After freeze-drying, the biomass carbon quantum dots were acquired and stored in a dark area. CQDs-1 and CQDs-2 were used to designate Salix wood powder preparation CQDs and lignin preparation CQDs, respectively.

2.2. Synthesis of N-Doped Wood-Based Carbon Quantum Dots

Synthesis of N-CQDs: Salix wood powder was chosen as the carbon source while urea served as the nitrogen source for the one-step hydrothermal synthesis of N-CQDs. After conducting experiment Section 2.1, it was determined that the optimal fluorescence performance of CQDs was achieved with the addition of 1.1 g of sallow wood powder. Consequently, adding sallow wood powder at 1.1 g and modifying the addition of urea, a nitrogen source, was selected to synthesize N-CQDs-1. The synthesis method followed the protocol outlined in Section 2.1. Specifically, 1, 2, or 3 g of nitrogen source were dissolved in 30 milliliters of deionized water. The resulting N-CQDs solid was obtained through a process of ultrasonication, heating, filtration, dialysis, and freeze-drying.

To improve the performance of N-CQDs-1 further, citric acid was utilized to activate the carbon source, enhancing its surface functional groups. The citric acid provided an acidic environment for the reaction, which promoted the hydrolysis of Salix wood powder and the degree of hydrothermal carbonization [23]. Moreover, more defect networks are generated on the surface of CQDs as defects of excitation energy trap and fluorescence recombination exciton trap, which enhance the FL. The ratio of citric acid to nitrogen

source addition was then adjusted to 1:2, 1:1, or 2:1 to obtain N-CQDs-2 with improved performance, utilizing the same synthesis method as Section 2.2.

2.3. Characterization of CQDs and N-CQDs

The morphology and particle size of the samples were characterized using Transmission Electron Microscopy (TEM; Model: JEOL-JEM 2100 F) and Nano Measurer. Fourier Transform Infrared Spectroscopy (FTIR; Model: Bruker INVENIO S) and X-ray Photoelectron Spectroscopy (XPS; Model: TD-3700) were used to characterize the samples. Functional groups were identified through fluorescence spectroscopy (model TD-3700). The excitation and emission fluorescence (PL) spectra of the samples were measured using a fluorescence spectrometer (Lengguang F98). The UV-Vis absorption spectra of the samples were measured with a UV spectrophotometer (model PE Lambda 850).

2.4. Effects of CQDs and N-CQDs on Photosynthetic Pigments

Soybean plants with a short growth cycle were chosen for this study, and CQDs and N-CQDs were sprayed on them to examine their impact on chlorophyll in photosynthetic pigments. The soybean variety used in the experiment was Zhonghuang 35. The planting environment was maintained at a temperature range of 23 to 26 degrees Celsius. The light source utilized was a general-purpose full-spectrum white light lamp with a light intensity of 12000LUX. The plants were subjected to an 18 h light and 6 h dark cycle. Soybean seeds were planted in pots and allowed to sprout. Uniformly grown soybean plants were then selected for cultivation over a period of 15 days. The aqueous dispersions of CQDs and N-CQDs were prepared with concentrations of 0, 5, 25, and 50 mg/L. We then evenly sprayed the samples on soybean foliage using a spray bottle. We carried out three group replicates for each treatment continuously for 7 days. After the treatments, we waited for a period of 10 days for the determination of photosynthesis pigments before harvesting.

The determination of photosynthetic pigment content was analyzed by calculating absorbance values to assess the effect of carbon quantum dots on pigment synthesis. In order to do this, 0.1 g of leaf samples were weighed and then immersed in 15 mL of 95% ethanol in a dark environment for 24 h. After the leaves had turned white, the supernatant was collected and analyzed for absorbance at 664 nm and 648 nm using a UV spectrophotometer (A_{664}, A_{648}). Chlorophyll a, chlorophyll b, and total chlorophyll content were then calculated using the following formulas.

$$\text{Chlorophyll a content (mg/L)} = 13.36A_{664} - 5.19A_{648} \quad (1)$$

$$\text{Chlorophyll b content (mg/L)} = 27.43A_{648} - 8.12A_{664} \quad (2)$$

$$\text{Total chlorophyll content (mg/L)} = 5.24A_{664} + 22.24A_{648} \quad (3)$$

2.5. Effect of CQDs and N-CQDs on Photosynthetic Activity

Extraction of chloroplasts: refer to the method of Pan et al. [8,24]. To extract chloroplasts, sucrose buffer (0.4 M (mol/L) sucrose, 0.01 M KCl, 0.03 M Na_2HPO_4, 0.02 M KH_2PO_4) was prepared with a pH of 7.3, then refrigerated at 4 °C. The mortar and sucrose buffer were also pre-cooled in the refrigerator after preparation. The leaves were weighed and ground with a suitable amount of mortar in the presence of 30 mL of sucrose buffer solution. The resulting mixture was filtered through gauze and collected in a light-protected centrifuge tube in order to obtain the crude chloroplast extract. The initial step of the experiment involved centrifuging the crude chloroplast extract at 1000 rpm for 3 min. Following this, the collected precipitate at the bottom was discarded, and the remaining supernatant was subjected to further centrifugation at 3000 rpm for 5 min to obtain the second precipitate. Finally, the supernatant after the second centrifugation was subjected to another round of centrifugation at 3000 rpm for 5 min to collect the third precipitate. The precipitate collected was redispersed in sucrose buffer to obtain the chloroplast suspension. All the aforementioned procedures were carried out under dark conditions at 0–4 °C.

The concentration of chloroplast suspension was determined by mixing 1 mL of suspension with 49 mL of acetone and measuring the absorbance of the mixture at 652 nm. The formula was calculated as follows.

$$\text{chloroplast (vein) content (mg/L) } C = OD_{652} \times 1000/34.5 \quad (4)$$

Hill Reaction: The purpose of the Hill reaction is to measure the rate of electron transfer in Photosystem II during photosynthesis. To express this, the rate of reduction of 2,6-Di-chloropheno-lindopheno (DCPIP) is used. A mixture of chloroplasts (5 mg/L), N-CQDs (5 mg/L), and CQDs (5 mg/L) in a sucrose buffer was prepared and allowed to sit for 5 min. Next, 60 µmol/L DCPIP was carefully added dropwise to the mixture to ensure sufficient mixing for 1 min. A control setup was included without chloroplasts. Photosynthesis was determined by measuring the solution's absorbance at 600 nm after a specified exposure time to light at 0, 1, 2, 3, 4, and 5 min. The reaction's kinetics were assessed by monitoring the absorption variance, while the electron reduction velocity was measured as outlined in reference [25].

3. Results and Discussion

3.1. Characterization of CQDs and N-CQDs

3.1.1. TEM Morphology Analysis

Figure 2 displays transmission electron microscope images of N-CQDs produced through a one-step hydrothermal method, providing insights into their morphology and microstructure. As depicted in Figure 3a, the N-CQDs exhibited regular spherical structures and excellent dispersion, aligning with the previously reported results of [23]. The histogram of particle size distribution was obtained through the counting of about 60 points (inset of Figure 2a). The results indicate a uniform distribution in the diameters of these points, ranging between 0.5 and 4.5 nm, with a mean size of 2.19 nm and a standard deviation of 0.85 nm. The HRTEM image in the inset of Figure 2b demonstrates the crystal quality of the N-CQDs. The N-CQDs exhibit a nearly circular shape, and their well-defined lattice stripes are prominently visible. The lattice stripe spacing of the N-CQDs is 0.21 nm. This aligns with the graphite (100) diffraction surface and suggests a single-crystal graphitic carbon lattice structure [18].

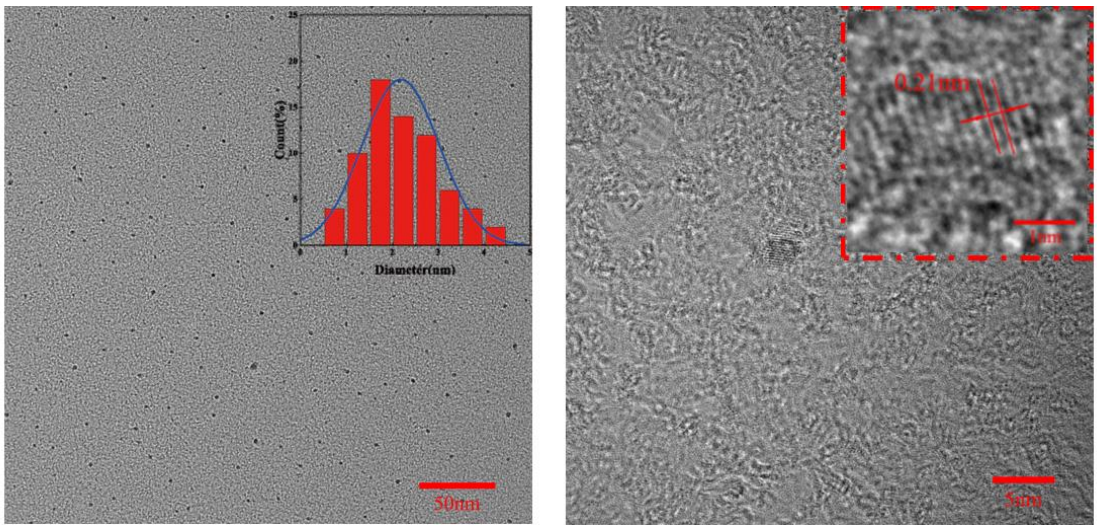

(**a**) (**b**)

Figure 2. (**a**) TEM of N-CQDs; (**b**) HRTEM of N-CQDs.

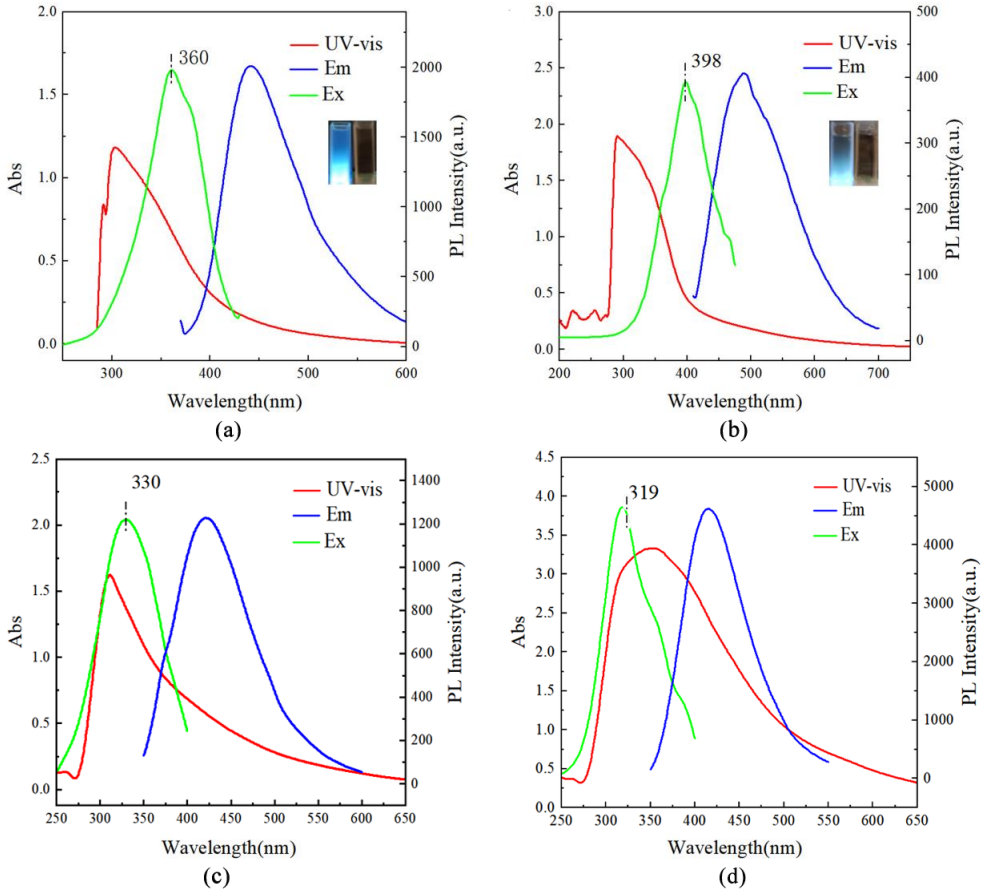

Figure 3. Optical properties of CQDs and N-CQDs (**a**) UV and fluorescence spectra of CQDs-1; (**b**) UV and fluorescence spectra of CQDs-2; (**c**) UV and fluorescence spectra of N-CQDs-1; (**d**) UV and fluorescence spectra of N-CQDs-2.

3.1.2. Optical Performance Analysis

Photoluminescence (PL) is a notable characteristic of CQDs. Optical absorption peaks of CQDs in the UV-visible wavelength range are displayed in Figure 3a,b. Both CQDs-1 and CQDs-2 UV-Vis absorption spectra show significant peaks at 303 nm and 291 nm, respectively. These peaks are predominantly correlated with the n-π* and π-π* electron transitions of the C=O and C=C bonds [26]. Comparing the UV-vis absorption spectra of N-CQDs after urea-doped Salix wood powder, as shown in Figure 3c,d, reveals pronounced absorption peaks at 310 nm and 350 nm. These peaks are a result of the n-π* and π-π* electron transitions of the C=O bond and C=C bond [27]. The photographs in Figure 3a,b illustrate that the CQDs and N-CQDs solutions prepared in this study emit strong blue photoluminescence under UV radiation at 365 nm. The most effective excitation wavelengths for CQDs-1, CQDs-2, N-CQDs-1, and N-CQDs-2 are 360 nm, 398 nm, 330 nm, and 319 nm, respectively, with corresponding maximum emission wavelengths of 440 nm, 489 nm, 420 nm, and 414 nm, respectively.

Figure S1a displays the fluorescence emission spectra of Salix wood powder CQDs. The results indicate that fluorescence intensity is highest when 1.1–1.3 g of carbon source is added, and based on performance and experimental cost considerations, we selected 1.1 g of carbon source for the next step of the experiment. Figure S1b displays the fluorescence emission spectra of nitrogen-doped carbon dots (N-CQDs) produced from Salix wood powder doped with urea, and urea added after citric acid activation of Salix wood powder. It is evident that fluorescence intensity improves following citric acid activation. Consequently, N-CQDs with a urea citrate addition ratio of 1:2 were employed to examine their impact on photosynthesis. Furthermore, the N-CQDs that were obtained exhibit excitation-dependent

emission spectra consistent with prior findings [28–35]. Upon increasing the excitation wavelength from 300 nm to 400 nm, there was a red-shift in fluorescence emission peaks, as well as a first increase in fluorescence intensity followed by a gradual decrease. The emission peaks for N-CQDs-1 and N-CQDs-2 dispersions are observed to gradually shift from 417 nm to 479 nm (Figure S1c) and from 415 nm to 473 nm (Figure S1d), respectively. These findings suggest that there is a gradual red shift in the dispersion. This photoluminescence emission range (417–479 nm, 415–473 nm) provides evidence for similar quantum effects and emission traps, with a concentrated size distribution on the surface of N-CQDs. This result is in accordance with the TEM findings (Figure 2) and indicates that the N-CQDs exhibit consistent and predictable behavior. The functional groups present on the surface of CQDs and N-CQDs [36,37] cause variations in energy levels associated with different surface states. This led to the further analysis of the surface functional groups of CQDs and N-CQDs in conjunction with FTIR.

3.1.3. FTIR Analysis

Fourier transform infrared (FT-IR) spectroscopy was utilized to analyze the molecules' structures and chemical composition of CQDs and N-CQDs. As illustrated in Figure S2a, the tendency and defining peaks of sandwillow wood powder and its CQDs-1 counterpart are essentially identical, signifying the retention of sandwillow wood powder's primary backbone structure. The absorption bands at 3337 cm^{-1}, 2905 cm^{-1}, and 1592 cm^{-1} result from the stretching vibration of the O–H bond, the vibration of the C–H bond, and the vibration of the C=C bond, respectively. The vibration of the C=C bond suggests the existence of multiple conjugated groups, which is a key factor in the luminescence of CQDs. The peaks observed at 1232 cm^{-1} and 1160 cm^{-1} were unequivocally attributed to the stretching vibrations of C–O and C–O–C, respectively [38]. In Figure S2b, CQDs-1 derived from Salix wood powder and urea-doped N-CQDs-1 and N-CQDs-2 are depicted, which correspond to Figure S2a the absorption bands at 3346 cm^{-1}, 2914 cm^{-1}, and 1578 cm^{-1} are the result of the O–H bond stretching vibration, C–H bond vibration, and C=C bond vibration, respectively. The peaks at 1200 cm^{-1} and 1115 cm^{-1} correspond to C–O and C–O–C stretching vibrations, respectively. The presence of a C–N bond peak at 1409 cm^{-1} in the spectrum of urea-doped carbon quantum dots indicates successful nitrogen doping [39,40].

3.1.4. XPS Analysis

The chemical composition of sample N-CQDs-2 was analyzed using x-ray photoelectron spectroscopy (XPS). The XPS spectra, as depicted in Figure S3a, indicate distinct peaks at 285, 400, and 532 eV that match with C1s, N1, and O1s, respectively. The elemental composition of N-CQDs-2 is 80.45% carbon, 16.68% oxygen, and 2.88% nitrogen. To analyze the bonding configuration of carbon, oxygen, and nitrogen in N-CQDs-2, their respective spectra (C1s, N1, and O1s) were deconvoluted. The C1s spectrum (Figure S3b) shows that the peaks at 284.7, 285.1, and 287.7 eV correspond to C–C/C=C, C–N, and C–O bonds, respectively [41]. The O1s spectrum (Figure S3c) of N-CQDs-2 exhibited two peaks at 533.0 and 532.3 eV for C–OH/C–O–C and O–H bonds, respectively. Moreover, the N1s spectrum (Figure S3d) of N-CQDs-2 displayed three N-related bonds at 399.3, 401.2, and 400.4 eV for C–N–C, N–H, and N–(C)3, correspondingly [26]. The nitrogen-doped, carbon-rich polymer nanodots designated as N-CQDs-2 have been successfully prepared. This was established through the presence of C–N bonds at 1409 cm^{-1} in the FTIR spectrum [42].

3.2. Analysis of Photosynthetic Pigment Content

Chlorophyll, a crucial pigment in photosynthesis, captures light energy during the light reaction. Heightened levels of chlorophyll intensify light absorption efficiency and the production of carbohydrates in plant photosynthesis. The chlorophyll content was measured through UV spectrophotometry. Compared with the blank control, the chlorophyll contents including chlorophyll a and chlorophyll b of soybean leaves treated with

CQDs and N-CQDs showed an increase, as shown in Figure 4. The CQDs concentrations of 5 mg/L, 25 mg/L, and 50 mg/L demonstrated a promoting and increasing trend, while N-CQDs of 5 mg/L and 25 mg/L also displayed a promotional effect. However, the promotional effect of 50 mg/L was more reduced compared to that of 5 mg/L and 25 mg/L, resulting in a more decreasing promotional effect. When comparing the concentration of CQDs and N-CQDs solutions at a low concentration, it was found that N-CQDs had a better promotional effect. In the N-CQDs 25 mg/L treated group, the chlorophyll content increased by 35.6% compared to the untreated group. However, this promotional effect was reduced at high concentrations. Despite this, the overall trend of promotion indicated that the presence of CQDs and N-CQDs is conducive to increasing the chlorophyll content of soybean plants [43]. The rate of photosynthesis accelerates with an increase in chlorophyll content as there is a positive correlation between them [44]. CQDs and N-CQDs capture light, assisting the chloroplast photosystem in oxidizing water molecules, leading to the capture of more light energy. Compared to natural chloroplasts, the electron transport chain theoretically produces more electrons, which significantly enhances photosynthetic activity [45]. Consequently, in the next set of experiments, it will be further investigated whether CQDs and N-CQDs participate in generating more electrons in the photosynthetic electron transport chain.

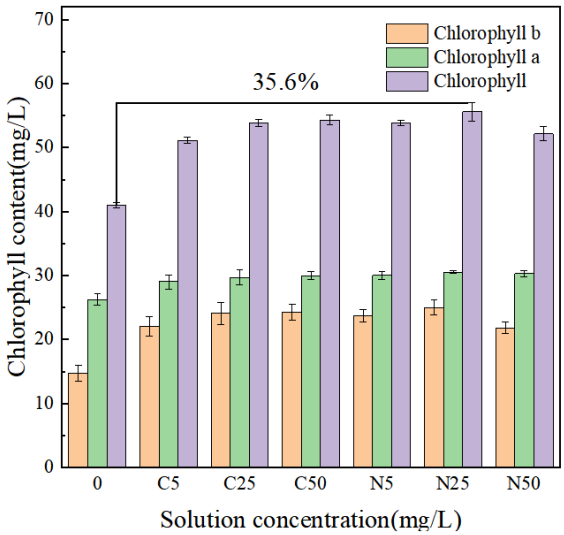

Figure 4. Chlorophyll content graph (0: No treatment solution containing CQDs or N-CQDs at a concentration of 0 mg/L was added. C5: Add a treatment solution containing CQDs at a concentration of 5 mg/L. C25: Add a treatment solution containing CQDs at a concentration of 25 mg/L. C50: Add a treatment solution containing CQDs at a concentration of 50 mg/L. N5: Add a treatment solution containing N-CQDs at a concentration of 5 mg/L. N25: Add a treatment solution containing N-CQDs at a concentration of 25 mg/L. N50: Add a treatment solution containing N-CQDs at a concentration of 50 mg/L).

3.3. Measurement of Photosynthetic Activity

The Hill reaction facilitates electron transfer from photosystem II (PSII) to photosystem I (PSI), and its efficacy is determined by the rate of reduction of DCPIP [46]. Our experiments were designed to examine whether chloroplasts can utilize blue light converted from UV absorption by CQDs and N-CQDs for photosynthesis. We aimed to investigate the effects of observing the CQDs and N-CQDs complexes with chloroplasts on the reduction pattern of DCPIP as compared to chloroplasts alone. According to Figure 5, the use of CQDs and N-CQDs in the chloroplast DCPIP complex decreased significantly, increasing the rate of electron transfer in the photosynthetic electron transport chain [47]. Consequently, it can be inferred that chloroplasts absorbed blue light, which was converted by CQDs and N-CQDs to enhance photosynthetic activity, promoting photosynthesis. Notably, the com-

plexes of N-CQDs and chloroplasts showed higher DCPIP reduction rates, suggesting that N-CQDs produce more electrons than CQDs [48,49], which may be due to N doping that promotes the separation of photoexcited electron-hole pairs.

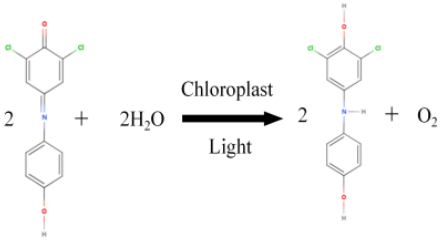

(**a**)

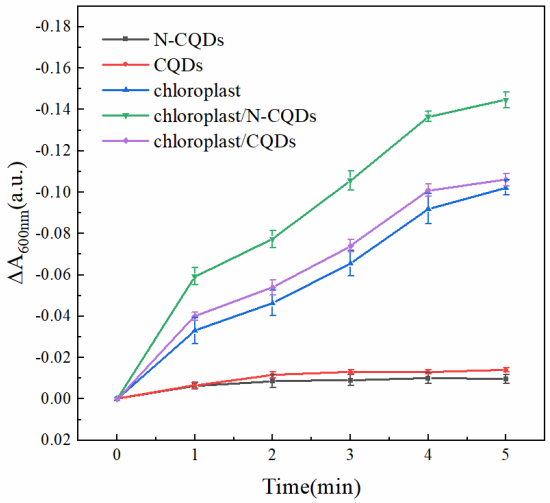

(**b**)

Figure 5. Photosynthetic activity of CQDs, N-CQDs, chloroplasts, CQDs chloroplast complexes, N-CQDs chloroplast complexes (**a**) Hill reaction equation; (**b**) DCPIP reduction rate plot.

4. Conclusions

In conclusion, in this paper, CQDs were prepared by a simple, green, and environmentally friendly hydrothermal method using Salix wood powder, and N-CQDs were successfully prepared by urea doping. Salix wood powder-based CQDs and N-CQDs have good water solubility, fluorescence, and optical stability. The use of this material as a light-trapping agent enables chloroplasts, which are unable to independently utilize UV light, to take advantage of it. Additionally, CQDs and N-CQDs can absorb and convert UV light into blue light, which can be directly utilized by chloroplasts in an effective manner. The research involved cultivating CQDs and N-CQDs soybean plants to enhance the chlorophyll content of photosynthetic pigments. Additionally, CQDs and N-CQDs were mixed individually with living chloroplasts to create CQDs and N-CQDs chloroplast complexes, which were then compared with single chloroplasts. As a result, the efficiency of photosynthetic electron transfer improved significantly. Salix wood flour-based CQDs and N-CQDs were found to enhance the utilization of light energy by chloroplasts, thereby promoting photosynthesis.

Supplementary Materials: The following supporting information can be downloaded at: https://www.mdpi.com/article/10.3390/coatings14040417/s1, Figure S1: Emission spectra of CQDs-1 (both excited at the optimal excitation wave of 360 nm); (b) Emission spectra of N-CQDs-1 and N-CQDs-2 (excited at the optimal excitation wave of 330 nm and 319 nm, respectively); (c) Emission spectra of N-CQDs-1 (excitation wavelengths of 300 nm-400 nm); (d) Emission spectra of N-CQDs-2 (excitation wavelengths of 300 nm-400 nm). Figure S2: (a) FTIR of CQDs; (b) FTIR of N-CQDs. Figure S3: (a) XPS spectra of N-CQDs; (b) C1s spectra of N-CQDs; (c) O1s spectra of N-CQDs; (d) N1s spectra of N-CQDs.

Author Contributions: Y.F.: designed this study, performed experiments, analyzed the data, and wrote the manuscript. H.X.: performed experiments, analyzed the data. Q.G.: methodology and experimentation. D.Y.: analyzed the data. Y.P.: methodology and experimentation. Z.X.: conceptualization, methodology, resources, revised the manuscript. All authors have read and agreed to the published version of the manuscript.

Funding: This work was supported by the National Natural Science Foundation of China (31860187).

Institutional Review Board Statement: Not applicable.

Informed Consent Statement: Not applicable.

Data Availability Statement: The data used to support the findings of this study are available from the corresponding author upon request.

Conflicts of Interest: The authors declare no conflicts of interest.

References

1. Gielen, D.; Boshell, F.; Saygin, D.; Bazilian, M.D.; Wagner, N.; Gorini, R. The Role of Renewable Energy in the Global Energy Transformation. *Energy Strategy Rev.* **2019**, *24*, 38–50. [CrossRef]
2. Wang, Q.; Pornrungroj, C.; Linley, S.; Reisner, E. Strategies to Improve Light Utilization in Solar Fuel Synthesis. *Nat. Energy* **2022**, *7*, 13–24. [CrossRef]
3. Gitelson, A.A.; Peng, Y.; Arkebauer, T.J.; Schepers, J. Relationships between Gross Primary Production, Green LAI, and Canopy Chlorophyll Content in Maize: Implications for Remote Sensing of Primary Production. *Remote Sens. Environ.* **2014**, *144*, 65–72. [CrossRef]
4. Gilbert, M.E.; Zwieniecki, M.A.; Holbrook, N.M. Independent Variation in Photosynthetic Capacity and Stomatal Conductance Leads to Differences in Intrinsic Water Use Efficiency in 11 Soybean Genotypes before and during Mild Drought. *J. Exp. Bot.* **2011**, *62*, 2875–2887. [CrossRef] [PubMed]
5. Maurino, V.G.; Weber, A.P.M. Engineering Photosynthesis in Plants and Synthetic Microorganisms. *J. Exp. Bot.* **2013**, *64*, 743–751. [CrossRef] [PubMed]
6. Maxwell, K.; Johnson, G.N. Chlorophyll Fluorescence—A Practical Guide. *J. Exp. Bot.* **2000**, *51*, 659–668. [CrossRef] [PubMed]
7. Wu, W.; Zhang, Z.; Dong, R.; Xie, G.; Zhou, J.; Wu, K.; Zhang, H.; Cai, Q.; Lei, B. Characterization and Properties of a $Sr_2Si_5N_8$:Eu^{2+}-Based Light-Conversion Agricultural Film. *J. Rare Earths* **2020**, *38*, 539–545. [CrossRef]
8. Pavlov, S.A.; Sherstneva, N.E.; Koryakin, S.L.; Maksimova, E.Y.; Makovetskiy, V.V.; Krikushenko, V.V.; Antipov, E.M. Features of Light Conversion Process with Covering Materials Containing Quantum Dots and Their Application in Agriculture. *Nano Hybrids Compos.* **2017**, *13*, 162–175. [CrossRef]
9. Dong, R.; Li, Y.; Li, W.; Zhang, H.; Liu, Y.; Ma, L.; Wang, X.; Lei, B. Recent Developments in Luminescent Nanoparticles for Plant Imaging and Photosynthesis. *J. Rare Earths* **2019**, *37*, 903–915. [CrossRef]
10. Nuccio, M.L.; Potter, L.; Stiegelmeyer, S.M.; Curley, J.; Cohn, J.; Wittich, P.E.; Tan, X.; Davis, J.; Ni, J.; Trullinger, J.; et al. Strategies and Tools to Improve Crop Productivity by Targeting Photosynthesis. *Philos. Trans. R. Soc. B Biol. Sci.* **2017**, *372*, 20160377. [CrossRef]
11. Gun'ko, Y.K.; Moloney, M.M.; Gallagher, S.; Govan, J.; Hanley, C. New Quantum Dot Sensors. In Proceedings of the Annual SPIE Defense, Security, and Sensing Conference, Orlando, FL, USA, 5–9 April 2010.
12. Zhao, M.-X.; Zeng, E.-Z. Application of Functional Quantum Dot Nanoparticles as Fluorescence Probes in Cell Labeling and Tumor Diagnostic Imaging. *Nanoscale Res. Lett.* **2015**, *10*, 171. [CrossRef] [PubMed]
13. de Dios, A.S.; Díaz-García, M.E. Multifunctional Nanoparticles: Analytical Prospects. *Anal. Chim. Acta* **2010**, *666*, 1–22. [CrossRef] [PubMed]
14. Ünlü, C.; Budak, E.; Kestir, S.M. Altering Natural Photosynthesis through Quantum Dots: Effect of Quantum Dots on Viability, Light Harvesting Capacity and Growth of Photosynthetic Organisms. *Funct. Plant Biol.* **2022**, *49*, 444–451. [CrossRef] [PubMed]
15. Rakovich, A.; Donegan, J.F.; Oleinikov, V.; Molinari, M.; Sukhanova, A.; Nabiev, I.; Rakovich, Y.P. Linear and Nonlinear Optical Effects Induced by Energy Transfer from Semiconductor Nanoparticles to Photosynthetic Biological Systems. *J. Photochem. Photobiol. C Photochem. Rev.* **2014**, *20*, 17–32. [CrossRef]
16. Li, Y.; Xu, X.; Wu, Y.; Zhuang, J.; Zhang, X.; Zhang, H.; Lei, B.; Hu, C.; Liu, Y. A Review on the Effects of Carbon Dots in Plant Systems. *Mater. Chem. Front.* **2020**, *4*, 437–448. [CrossRef]
17. Xu, X.; Ray, R.; Gu, Y.; Ploehn, H.J.; Gearheart, L.; Raker, K.; Scrivens, W.A. Electrophoretic Analysis and Purification of Fluorescent Single-Walled Carbon Nanotube Fragments. *J. Am. Chem. Soc.* **2004**, *126*, 12736–12737. [CrossRef] [PubMed]
18. Das, R.; Bandyopadhyay, R.; Pramanik, P. Carbon Quantum Dots from Natural Resource: A Review. *Mater. Today Chem.* **2018**, *8*, 96–109. [CrossRef]
19. Ghosal, K.; Ghosh, A. Carbon Dots: The next Generation Platform for Biomedical Applications. *Mater. Sci. Eng. C* **2019**, *96*, 887–903. [CrossRef] [PubMed]
20. Sun, Y.-P.; Zhou, B.; Lin, Y.; Wang, W.; Fernando, K.A.S.; Pathak, P.; Meziani, M.J.; Harruff, B.A.; Wang, X.; Wang, H.; et al. Quantum-Sized Carbon Dots for Bright and Colorful Photoluminescence. *J. Am. Chem. Soc.* **2006**, *128*, 7756–7757. [CrossRef]
21. Li, Y.-D.; Xu, X.-K.; Li, W.; Hu, C.-F.; Zhuang, J.-L.; Zhang, X.-J.; Lei, B.-F.; Liu, Y.-L. Progress of fluorescent carbon spot regulation of plant photosynthesis. *J. Lumin.* **2021**, *42*, 1172–1181.
22. Dots Xia, C.; Zhu, S.; Feng, T.; Yang, M.; Yang, B. Evolution and Synthesis of Carbon Dots: From Carbon Dots to Carbonized Polymer Dots. *Adv. Sci.* **2019**, *6*, 1901316.

23. Li, X.; Liu, X.; Su, Y.; Jiang, T.; Li, D.; Ma, X. Green Synthesis of Carbon Quantum Dots from Wasted Enzymatic Hydrolysis Lignin Catalyzed by Organic Acids for UV Shielding and Antioxidant Fluorescent Flexible Film. *Ind. Crops Prod.* **2022**, *188*, 115568. [CrossRef]
24. Wang, C.; Hu, T.; Thomas, T.; Song, S.; Wen, Z.; Wang, C.; Song, Q.; Yang, M. Surface State-Controlled C-Dot/C-Dot Based Dual-Emission Fluorescent Nanothermometers for Intra-Cellular Thermometry. *Nanoscale* **2018**, *10*, 21809–21817. [CrossRef] [PubMed]
25. Li, Y.; Xu, X.; Lei, B.; Zhuang, J.; Zhang, X.; Hu, C.; Cui, J.; Liu, Y. Magnesium-Nitrogen Co-Doped Carbon Dots Enhance Plant Growth through Multifunctional Regulation in Photosynthesis. *Chem. Eng. J.* **2021**, *422*, 130114. [CrossRef]
26. Zou, J.-P.; Wang, L.-C.; Luo, J.; Nie, Y.-C.; Xing, Q.-J.; Luo, X.-B.; Du, H.-M.; Luo, S.-L.; Suib, S.L. Synthesis and Efficient Visible Light Photocatalytic H_2 Evolution of a Metal-Free g-C_3N_4/Graphene Quantum Dots Hybrid Photocatalyst. *Appl. Catal. B Environ.* **2016**, *193*, 103–109. [CrossRef]
27. Shi, Y.; Liu, X.; Wang, M.; Huang, J.; Jiang, X.; Pang, J.; Xu, F.; Zhang, X. Synthesis of N-Doped Carbon Quantum Dots from Bio-Waste Lignin for Selective Irons Detection and Cellular Imaging. *Int. J. Biol. Macromol.* **2019**, *128*, 537–545. [CrossRef] [PubMed]
28. Arumugam, N.; Kim, J. Synthesis of Carbon Quantum Dots from Broccoli and Their Ability to Detect Silver Ions. *Mater. Lett.* **2018**, *219*, 37–40. [CrossRef]
29. Li, X.; Wang, H.; Shimizu, Y.; Pyatenko, A.; Kawaguchi, K.; Koshizaki, N. Preparation of Carbon Quantum Dots with Tunable Photoluminescence by Rapid Laser Passivation in Ordinary Organic Solvents. *Chem. Commun.* **2010**, *47*, 932–934. [CrossRef] [PubMed]
30. Lu, J.; Yang, J.; Wang, J.; Lim, A.; Wang, S.; Loh, K.P. One-Pot Synthesis of Fluorescent Carbon Nanoribbons, Nanoparticles, and Graphene by the Exfoliation of Graphite in Ionic Liquids. *ACS Nano* **2009**, *3*, 2367–2375. [CrossRef]
31. Liu, H.; Ye, T.; Mao, C. Fluorescent Carbon Nanoparticles Derived from Candle Soot. *Angew. Chem. Int. Ed.* **2007**, *46*, 6473–6475. [CrossRef]
32. Chen, Z.; Zhao, Z.; Wang, Z.; Zhang, Y.; Sun, X.; Hou, L.; Yuan, C. Foxtail Millet-Derived Highly Fluorescent Multi-Heteroatom Doped Carbon Quantum Dots towards Fluorescent Inks and Smart Nanosensors for Selective Ion Detection. *New J. Chem.* **2018**, *42*, 7326–7331. [CrossRef]
33. Tyagi, A.; Tripathi, K.M.; Singh, N.; Choudhary, S.; Gupta, R.K. Green Synthesis of Carbon Quantum Dots from Lemon Peel Waste: Applications in Sensing and Photocatalysis. *RSC Adv.* **2016**, *6*, 72423–72432. [CrossRef]
34. Zhu, H.; Wang, X.; Li, Y.; Wang, Z.; Yang, F.; Yang, X. Microwave Synthesis of Fluorescent Carbon Nanoparticles with Electrochemiluminescence Properties. *Chem. Commun.* **2009**, 5118–5120. [CrossRef] [PubMed]
35. Chen, B.; Li, F.; Li, S.; Weng, W.; Guo, H.; Guo, T.; Zhang, X.; Chen, Y.; Huang, T.; Hong, X.; et al. Large Scale Synthesis of Photoluminescent Carbon Nanodots and Their Application for Bioimaging. *Nanoscale* **2013**, *5*, 1967–1971. [CrossRef] [PubMed]
36. Wang, C.; Shi, H.; Yang, M.; Yan, Y.; Liu, E.; Ji, Z.; Fan, J. Facile Synthesis of Novel Carbon Quantum Dots from Biomass Waste for Highly Sensitive Detection of Iron Ions. *Mater. Res. Bull.* **2020**, *124*, 110730. [CrossRef]
37. Tripathi, K.M.; Sonker, A.K.; Bhati, A.; Bhuyan, J.; Singh, A.; Singh, A.; Sarkar, S.; Sonkar, S.K. Large-Scale Synthesis of Soluble Graphitic Hollow Carbon Nanorods with Tunable Photoluminescence for the Selective Fluorescent Detection of DNA. *New J. Chem.* **2016**, *40*, 1571–1579. [CrossRef]
38. Lu, M.; Duan, Y.; Song, Y.; Tan, J.; Zhou, L. Green Preparation of Versatile Nitrogen-Doped Carbon Quantum Dots from Watermelon Juice for Cell Imaging, Detection of Fe^{3+} Ions and Cysteine, and Optical Thermometry. *J. Mol. Liq.* **2018**, *269*, 766–774. [CrossRef]
39. Wu, Z.L.; Zhang, P.; Gao, M.X.; Liu, C.F.; Wang, W.; Leng, F.; Huang, C.Z. One-Pot Hydrothermal Synthesis of Highly Luminescent Nitrogen-Doped Amphoteric Carbon Dots for Bioimaging from Bombyx Mori Silk—Natural Proteins. *J. Mater. Chem. B* **2013**, *1*, 2868–2873. [CrossRef] [PubMed]
40. Huang, Z.; Guo, B.; Zou, Y.; He, J.; Hu, C.; Zhuang, J.; Liu, Y. Different Kinds of Citric Acid Based Carbon Dots and Their Enhancement of the Growth of Italian Lettuce. *ACS Agric. Sci. Technol.* **2022**, *2*, 684–692. [CrossRef]
41. Yuan, S.-J. Lignin Extraction and Preparation of Carbon Quantum Dots and Applications. Master's Thesis, Guangdong University of Technology, Guangzhou, China, 2022.
42. Gan, J.; Wu, Y.; Yang, F.; Zhang, H.; Wu, X.; Wang, Y.; Xu, R. Wood-Cellulose Photoluminescence Material Based on Carbon Quantum Dot for Light Conversion. *Carbohydr. Polym.* **2022**, *290*, 119429. [CrossRef]
43. Si, M.; Zhang, J.; He, Y.; Yang, Z.; Yan, X.; Liu, M.; Zhuo, S.; Wang, S.; Min, X.; Gao, C.; et al. Synchronous and Rapid Preparation of Lignin Nanoparticles and Carbon Quantum Dots from Natural Lignocellulose. *Green Chem.* **2018**, *20*, 3414–3419. [CrossRef]
44. Wang, H.; Zhang, M.; Song, Y.; Li, H.; Huang, H.; Shao, M.; Liu, Y.; Kang, Z. Carbon Dots Promote the Growth and Photosynthesis of Mung Bean Sprouts. *Carbon* **2018**, *136*, 94–102. [CrossRef]
45. Ren, H.-X.; Liu, L.; Liu, C.; He, S.-Y.; Huang, J.; Li, J.-L.; Zhang, Y.; Huang, X.-J.; Gu, N. Physiological Investigation of Magnetic Iron Oxide Nanoparticles towards Chinese Mung Bean. *J. Biomed. Nanotechnol.* **2011**, *7*, 677–684. [CrossRef] [PubMed]
46. Tan, Z.; She, M.; Chen, Q.; Liu, L.; Cai, X.; Huang, Y.; Xiang, F. Impact of Dual-Emissive Carbon Dots on Growth and Physiological Indexes of Cucumber Seedlings. *Gesunde Pflanz.* **2022**, *74*, 695–704. [CrossRef]
47. Kopnov, F.; CoheN-Ofri, I.; Noy, D. Electron Transport between Photosystem II and Photosystem I Encapsulated in Sol–Gel Glasses. *Angew. Chem. Int. Ed.* **2011**, *50*, 12347–12350. [CrossRef] [PubMed]

48. Di, J.; Xia, J.; Chen, X.; Ji, M.; Yin, S.; Zhang, Q.; Li, H. Tunable Oxygen Activation Induced by Oxygen Defects in Nitrogen Doped Carbon Quantum Dots for Sustainable Boosting Photocatalysis. *Carbon* **2017**, *114*, 601–607. [CrossRef]
49. Tsai, K.-A.; Hsieh, P.-Y.; Lai, T.-H.; Tsao, C.-W.; Pan, H.; Lin, Y.-G.; Hsu, Y.-J. Nitrogen-Doped Graphene Quantum Dots for Remarkable Solar Hydrogen Production. *ACS Appl. Energy Mater.* **2020**, *3*, 5322–5332. [CrossRef]